Journal of ELECTRONIC MATERIALS, Vol. 48, No. 7, 2019
https://doi.org/10.1007/s11664-019-07190-x

Approach to Defect-Free Lifetime and High Electron Density in CdTe

S.K. SWAIN,[1,3] J.N. DUENOW,[2] S.W. JOHNSTON,[2] M. AMARASINGHE,[2] J.J. MCCOY,[1] W.K. METZGER,[2] and K.G. LYNN[1]

1.—Center for Materials Research, Washington State University, Pullman, WA 99164, USA. 2.—National Renewable Energy Laboratory, Golden, CO 80401, USA. 3.—e-mail: santosh@wsu.edu

Achieving simultaneously high carrier density and lifetime is important for II–VI semiconductor-based applications such as photovoltaics and infrared detectors; however, it is a challenging task. In this work, high purity CdTe single crystals doped with indium (In) were grown by vertical Bridgman melt growth under carefully controlled stoichiometry. Two-photon excitation time-resolved photoluminescence was employed to measure bulk recombination lifetime by eliminating surface recombination effects. By adjusting stoichiometry with post growth annealing, high-net free carrier density approaching 10^{18} cm^{-3} was achieved simultaneously with lifetime approaching the radiative limit by suppressing non-radiative recombination centers.

Key words: *n*-type CdTe, time resolved photoluminescence, carrier density, life time

INTRODUCTION

Simultaneously, high carrier density and lifetime are desirable for semiconductor device applications such as photovoltaics, lasers, LEDs, and conductive substrates for infrared detectors.[1] However, II–VI semiconductors such as CdTe exhibit self-compensation due to the relatively higher ionic nature of the II–VI bonding compared to III–V or Si semiconductors.

To form *n*-type material in CdTe, we seek to substitute indium on a Cd-vacancy to create a single donor In_{Cd}^{+}. In order to increase the Cd-vacancy concentration and indium solubility, bulk CdTe crystals were grown under Te-rich conditions. However, a challenge emerges because under the Te-rich condition, cadmium vacancies have a low formation energy, and excessive Cd vacancies can lead to electrical compensation.[2] For example, abundant cadmium vacancies create the identified donor-vacancy complex acceptor $(In_{Cd}^{+}\text{-}V_{Cd}^{-2})^{-}$, also known as A-centers, which compensates the desired In_{Cd}^{+} donor.[3] As a result, In-doped CdTe often results in nearly intrinsic electrical conductivity.[4]

In addition to shallow dopants, mid-gap states can play an active role in overall hole and electron density. For example, to achieve semi-insulating CdTe, the residual carrier concentration needs to be $< 10^{8}$ cm^{-3}, while unintentional impurities $\sim 10^{15}$ cm^{-3} are usually present even in high purity crystals not including hydrogen. Despite this, high resistivity has been obtained in undoped Te-rich CdTe.[5] A mechanism involving a mid-gap state has been successful in explaining the observed semi-insulating behavior, where the deep level is attributed to a doubly ionized state of a tellurium (Te_{Cd}^{+2}) antisite or its complexes.[5]

Consequently, there are very few reports on high ($> 10^{17}$ cm^{-3}) electron doping in CdTe.[6] High *n*-type CdTe has been reported by molecular beam epitaxy (MBE) and sputtering where the role of Cd overpressure has been emphasized.[7] However corresponding lifetime measurements were not performed. One recent study demonstrated high quality CdTe with both high lifetime and doping density by using iodine doping. However, the results

(Received August 27, 2018; accepted April 3, 2019; published online April 11, 2019)

were obtained in CdTe thin films grown by MBE on single crystal (CdTe, CdZnTe and InSb) substrates.[8] Additionally, non-stoichiometry related defects are known to be effective non-radiative recombination centers and responsible for short minority carrier lifetimes in CdTe.[9] Increased doping can also create extended defects; therefore, increased dopant concentration of shallow donors and acceptors sufficient to achieve electron or hole density $> 10^{18}$ cm^{-3} can also lead to increased recombination.[10,11] Furthermore, surfaces may interfere with accurate determination of bulk lifetimes.[12,13] To accurately determine the bulk CdTe lifetime independent of surface recombination in samples that are heavily doped, we apply sub-bandgap two-photon excitation single photon counting.[14] The results in this study demonstrate that stable free electron density $> 5 \times 10^{17}$ cm^{-3} can be obtained by Cd overpressure annealing, and the carrier lifetime transitions from defect dominated non-radiative mechanisms for low carrier density to more radiative limited lifetime in crystals with high carrier density.

EXPERIMENTAL PROCEDURE

Bulk CdTe crystals were melt-grown by the modified vertical Bridgman method by adding elemental indium ($\sim 8.7 \times 10^{18}$ cm^{-3}) to the CdTe melt. Excess Te in the amount of 1.45×10^{20} cm^{-3} was added to ensure Te-rich growth conditions and enhance In incorporation. Glow discharge mass spectrometry (GDMS) performed on the crystal indicates In atomic concentration of $\sim 3 \times 10^{18}$ cm^{-3}. Impurity analysis is important to understand if and which unintentional elements may contribute to observed carrier density and lifetime. Table I indicates unintentional impurity concentrations were fairly low (sub-ppm level) compared to the doping level. Impurities that are known to create deep levels (for example Ni, Cr, Sn) were not observed in the GDMS purity analysis.

Post-growth annealing under Cd overpressure conditions was performed at 700°C for 16 h on $(10 \times 10 \times 2)$ mm^3 polished crystals sealed in an evacuated quartz ampoule. Post-anneal cooling to room temperature was performed by quenching the samples from 700°C within seconds by immersing the ampoules in water. Some samples were slow-cooled to room temperature over a period of about 3 h. The electrical properties were insensitive to the cooling method, hence quenching was not critical to achieve optimal defect chemistry. Hall measurements were performed on as-grown and annealed crystals after polishing the surface and applying ohmic indium metal contacts.

Table I. Atomic concentration of unintentional impurities and indium dopant concentrations obtained by GDMS analysis on the CdTe:In crystal

Impurities	Atomic concentration (cm^{-3})
Na	2.3×10^{15}
Mg	4.8×10^{14}
Al	2.4×10^{14}
Si	3.6×10^{14}
Cu	9×10^{14}
In	3×10^{18}

The actual concentration may lie in the range of one half- to twofold of the value reported in the table, due to the uncertainty in GDMS measurements.

Time-resolved photoluminescence (TRPL) measurements were collected using a mode-locked, 200-femtosecond-pulse-width laser firing 1.1×10^6 pulses per second and a tunable-wavelength optical parametric amplifier. The wavelength was set to 640 nm for single photon excitation. A PicoQuant PicoHarp 300 time-correlated single-photon counting system collected the TRPL data. Two-photon excitation (2PE) generated carriers deep in the bulk by focusing the excitation below the top surface to measure bulk recombination mechanisms without surface recombination effects. The laser was tuned to 1120 nm, and the beam was focused within the sample to attain sufficient photon flux for two-photon absorption using a 20× or 40× microscope objective.

RESULTS AND DISCUSSION

Hall measurements on as-grown crystals indicate $\sim 3 \times 10^{13}$ cm^{-3} free electron density, which is nearly five orders of magnitude lower than the detected indium concentration, indicating electrical compensation. This CdTe self-compensation with shallow donors such as In, Al, and Cl has been observed in the literature, and is attributed to the A-center complex formation involving a substitutional donor, either on Cd or Te site with an isolated Cd vacancy.[15] Since the crystals were grown under Te-rich conditions, Cd vacancy formation is naturally promoted. The Te-rich condition also favors Te-antisite (Te_{Cd}) formation, which forms a deep level.[9,16] Other important complexes can be formed by vacancies bonding with antisites.[17] The semi-insulating behavior of CdTe over a wide doping range of shallow donors has been attributed to these deep levels pinning the Fermi level near the middle of the bandgap.[18]

Consequently, to achieve higher net carrier densities by extrinsic doping, the stoichiometry was adjusted at high temperature to prevent A-center formation. Several samples were post-growth annealed under Cd overpressure. Figure 1a indicates an axially cut CdTe:In crystal with visibly large single crystalline regions. A sample for GDMS was selected from near the middle region of the crystal to determine the average concentration of impurities and dopant. Figure 1b shows Hall measurements performed at three different regions along the axial direction in order to observe any

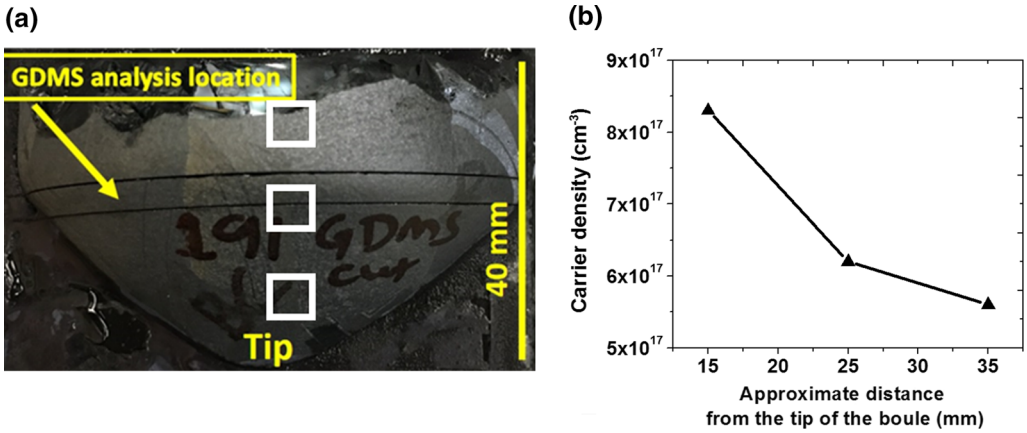

Fig. 1. (a) Picture of the large grained CdTe:In crystal grown by vertical Bridgman method. The location of sample for GDMS analysis and Hall measurements (squares) are also indicated. (b) Free carrier density measured on annealed samples from the selected locations of the crystal.

carrier density variation along the axial direction due to dopant segregation effects. The measured electron density on the annealed crystals at different axial locations ranged from 5.6×10^{17} cm^{-3} to 8.3×10^{17} cm^{-3}, indicating excellent uniformity and the absence of any significant segregation.

The crystal stoichiometry shift is inferred from depth-of-field infrared microscopy studies. Secondary phases of Te compositions (tellurium inclusions) are known to exist in CdTe crystals grown without any Cd partial pressure control.[19] These phases are classified into two categories based on their formation mechanism. Figure 2 shows an IR micrograph where the secondary phases can be observed as dark features. The relatively large particles shown in Fig. 2 that are several microns in diameter form during growth by the trapping of Te-rich melt droplets at the solid–liquid interface. These droplets are caused by instabilities triggered by interfacial thermal and compositional inhomogeneity. The melt gets increasingly enriched with Te as the growth progresses, due to preferential Cd evaporation because of its higher vapor pressure relative to Te. The second class of phases known as precipitates, which are typically observed by transmission electron microscopy (TEM), form due to the limited solid solubility of Te in the CdTe matrix.[20] Therefore, any excess Te in the CdTe solid precipitates out during post growth crystal cooling to room temperature. In either case, the second phase objects are consequences of the Te-rich growth stoichiometry.

After post-growth annealing under Cd overpressure, IR microscopy analysis reveals the size and density of second phases significantly decreased from 4.8×10^5 cm^{-3} to 2×10^4 cm^{-3}. Cd overpressure annealing reduces the overall volume percentage from 8.3×10^{-3}% to 2×10^{-4}%. The dissolution of secondary phases upon Cd diffusion during annealing, further confirms the Te composition of these phases, and is consistent with fewer V_{Cd} acceptors contributing to increased free electron density after annealing. Longer annealing times are

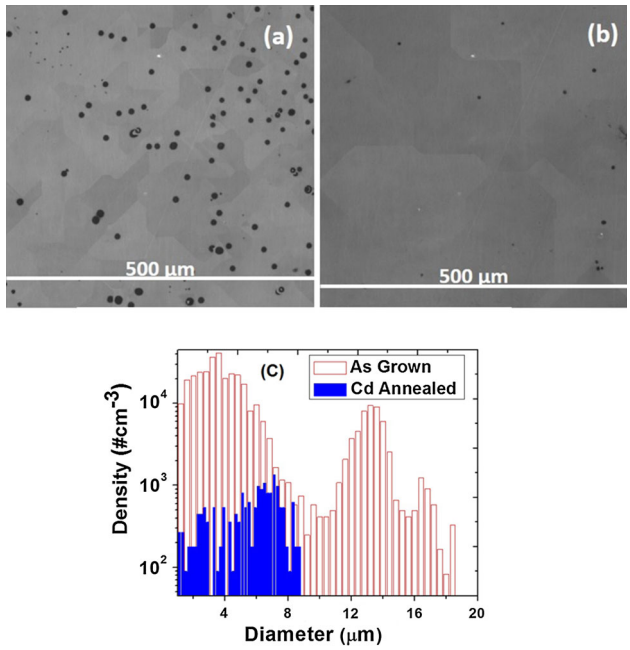

Fig. 2. Depth-of-field IR micrograph on the CdTe:In crystals (a) as-grown, (b) post-growth Cd annealed, and (c) density distribution of second phase particles before (hollow red) and after annealing (solid blue) (Color figure online).

necessary to further reduce inclusion size, and the reduced Te inclusion size and density is also desired for improved IR transmission for substrate applications.

Te inclusion sites are energetically favored to gain impurities.[21] Post-growth annealing to dissolve the inclusions can result in the release of these impurities to the matrix, which can be observed in GDMS measurements. Here, the possibility that such impurities govern the observed electrical behavior after annealing can be excluded based on the GDMS measured impurity concentrations. Impurity concentration determined by GDMS include overall impurities in the crystal including near second phases, and as seen in the table the concentration

of shallow levels in Table I, are much lower than the free electron density.

The experimentally determined minority carrier lifetime can be described by the equations,

$$1/\tau_{\text{eff}} = 1/\tau_{\text{S}} + 1/\tau_{\text{B}}, \quad (1)$$

and

$$1/\tau_{\text{B}} = 1/\tau_{\text{R}} + 1/\tau_{\text{SRH}} + 1/\tau_{\text{A}}, \quad (2)$$

where τ_{S} and τ_{B} are the surface and bulk lifetimes. The bulk recombination rate is given by the sum of radiative recombination rate (τ_{R}) and non-radiative processes such as Shockley–Read–Hall (τ_{SRH}) and Auger (τ_{A}). For non-degenerate semiconductors under low-injection conditions where the photoinjected carriers are less than the equilibrium electron density,

$$\tau_{\text{R}} = 1/(Bn) \quad (3)$$

and

$$\tau_{\text{A}} = 1/(Cn^2) \quad (4)$$

Here n, B, and C are the free-electron concentration, radiative recombination coefficient, and Auger coefficient, respectively. Several values for the CdTe radiative recombination coefficient have been reported in the literature,[22,23] here the value 1×10^{-10} cm^3/s is used.[24]

The bulk minority carrier lifetime measured by 2PE single photon counting for the as-grown and annealed crystals are 470 ns and 2.1 ns, respectively (Fig. 3). Based on the measured carrier density, the radiative lifetime is estimated to be 333 μs for the as-grown crystals, which is several orders of magnitude greater than the measured value, suggesting non-radiative decay as the dominant mechanism. Considering the high purity level of the crystals, the recombination may be caused by deep native defects such as Te antisite or dislocations. The etch pit density on similarly grown indium doped crystals are measured in the range (4–8) $\times$ 10^4 cm^{-2}. For the annealed crystals, the estimated radiative lifetime corresponding to the lowest (5.6×10^{17} cm^{-3}) and highest (8.3×10^{17} cm^{-3}) measured carrier densities are 18 ns and 12 ns, respectively. Hence, for these crystals, the observed bulk lifetime of 2.1 ns indicates the decay process is approaching the radiative limit. Figure 1c shows the expected radiatively limited lifetime as a function of free carrier density. Also shown in the plot are the experimentally measured lifetime in this work on samples before and after annealing. The lifetime in the annealed crystals approaching the defect-free radiative limit can be attributed to the annihilation of deep native defects by Cd overpressure annealing, consistent with the observation from electrical and IR measurements.

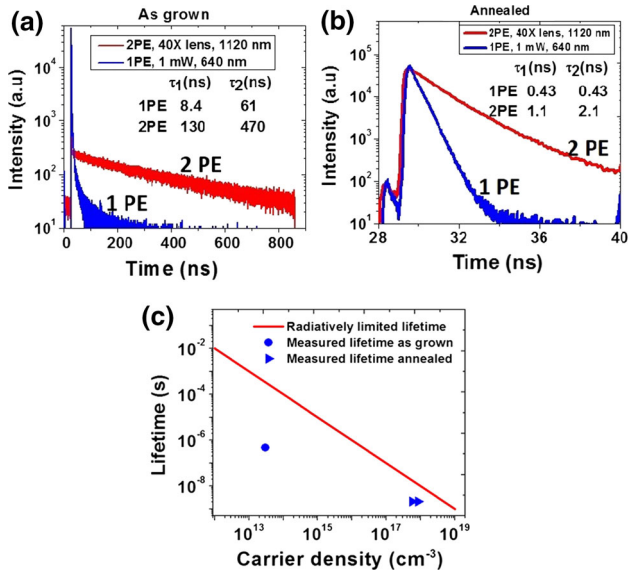

Fig. 3. Two-photon TRPL results indicating bulk lifetimes of (a) 470 ns for as-grown and (b) 2.1 ns for post growth Cd overpressure annealed CdTe:In. (c) Comparison of experimentally measured lifetime with the radiatively limited lifetime. The post-anneal measured lifetime of 2.1 ns is shown assuming the lowest (5.6×10^{17} cm^{-3}) and highest (8.3×10^{17} cm^{-3}) measured carrier densities by Hall measurement.

The CdTe Auger recombination coefficient has not been reported in the literature. The value reported for GaAs is $C \sim 1 \times 10^{-31}$ cm^6/s,[25] which is similar in bandgap to CdTe. Using this value for C, for the measured lifetime of 2.1 ns, the carrier density should be nearly 7×10^{19} cm^3 for the Auger process to be effective, which is nearly two orders of magnitude higher than the carrier densities in our crystals. It is unlikely that the recombination in these crystals is caused by intrinsic Auger mechanisms, and further studies are needed to establish CdTe Auger recombination values.

Surface recombination velocity (S) was estimated using the equation[26]

$$\tau_1 = \tau_{\text{B}}/(1 + \alpha S \tau_{\text{B}}) \quad (5)$$

where α is the CdTe absorption coefficient, and τ_1 is the decay rate in the initial section of the 1PE decay curve, dominated by surface recombination. For the as-grown and annealed samples, the surface recombination velocity, S, is estimated to be $\sim 2.3 \times 10^3$ cm/s and $\sim 4.6 \times 10^4$ cm/s, respectively. This order of magnitude difference could be caused by surface damage induced by high temperature Cd annealing as well as the migration of extended defects and dislocations to the surface.

CONCLUSIONS

In summary, a two-step strategy involving incorporation of indium by Te-rich bulk growth followed by activation by Cd overpressure annealing successfully obtains free electron density $> 5 \times 10^{17}$ cm^{-3}. At the same time, the Cd overpressure

reduces secondary phases of Te composition significantly and shifts the stoichiometry to reduce Te_{Cd} antisites. This leads to bulk lifetimes of 2.1 ns approaching the radiative limit. However, the annealing also appears to increase the surface recombination velocity here. The reduced size and density of second phase extended defects in CdTe with large carrier density makes the material suitable for conductive IR transparent substrates. Furthermore, the bulk growth methods provide a path to manufacture large quantities of *n*-type CdTe for electro-optical applications.

ACKNOWLEDGMENTS

This work was authored in part by the National Renewable Energy Laboratory, operated by Alliance for Sustainable Energy, LLC, for the U.S. Department of Energy (DOE) under Contract No. DE-AC36-08GO28308. This material is based in part upon work supported by the U.S. Department of Energy's Office of Energy Efficiency and Renewable Energy (EERE) under Solar Energy Technologies Office (SETO) Agreement 34353. The views expressed in the article do not necessarily represent the views of the DOE or the U.S. Government. The U.S. Government retains and the publisher, by accepting the article for publication, acknowledges that the U.S. Government retains a nonexclusive, paid-up, irrevocable, worldwide license to publish or reproduce the published form of this work, or allow others to do so, for U.S. Government purposes.

REFERENCES

1. M.O. Reese, A. Kanevce, T.M. Barnes, S.A. Jensen, and W.K. Metzger, *J. Appl. Phys.* 121, 214506 (2017).
2. S.-H. Wei and S.B. Zhang, *Phys. Rev. B.* 66, 155211 (2002).
3. W. Stadler, D.M. Hofmann, H.C. Alt, T. Muschik, B.K. Meyer, E. Weigel, G. Müller-Vogt, M. Salk, E. Rupp, and K.W. Benz, *Phys. Rev. B.* 51, 10619 (1995).
4. S. Seto, K. Suzuki, V.N. Abastillas Jr., and K. Inabe, *J. Cryst. Growth* 214, 974 (2000).
5. N. Krsmanovic, K.G. Lynn, M.H. Weber, R. Tjossem, Th. Gessmann, Cs. Szeles, E.E. Eissler, J.P. Flint, and H.L. Glass, *Phys. Rev. B.* 62, 16279 (2000).
6. B. Segall, M.R. Lorenz, and R.E. Halsted, *Phys. Rev.* 129, 2471 (1963).
7. M. Becerril, O. Zelaya-Angel, R. RamÍrez-Bon, F.J. Espinoza-Beltrán, and K. González-Hernández, *Appl. Phys. Lett.* 70, 452 (1997).
8. O.S. Ogedengbe, C.H. Swartz, P.A.R.D. Jayathilaka, J.E. Petersen, S. Sohal, E.G. LeBlanc, M. Edirisooriya, K.N. Zaunbrecher, A. Wang, T.M. Barnes, and T.H. Myers, *J. Electron. Mater.* 46, 5424 (2017).
9. J. Ma, D. Kuciauskas, D. Albin, R. Bhattacharya, M. Reese, T. Barnes, J.V. Li, T. Gessert, and S.-H. Wei, *Phys. Rev. Lett.* 111, 067402 (2013).
10. J.-H. Yang, W.K. Metzger, and S.-H. Wei, *Appl. Phys. Lett.* 111, 042106 (2017).
11. S. Farrell, T. Barnes, W.K. Metzger, J.H. Park, R. Kodama, and S. Sivananthan, *J. Electron. Mater.* 44, 3202 (2015).
12. M.O. Reese, C.L. Perkins, J.M. Burst, S. Farrell, T.M. Barnes, S.W. Johnston, D. Kuciauskas, T.A. Gessert, and W.K. Metzger, *J. Appl. Phys.* 118, 155305 (2015).
13. M.O. Reese, J.M. Burst, C.L. Perkins, A. Kanevce, S.W. Johnston, D. Kuciauskas, T.M. Barnes, and W.K. Metzger, *IEEE J. Photovolt.* 5, 382 (2015).
14. D. Kuciauskas, A. Kanevce, J.M. Burst, J.N. Duenow, R. Dhere, D.S. Albin, D.H. Levi, and R.K. Ahrenkiel, *IEEE J. Photovolt.* 3, 1319 (2013).
15. D.M. Hofmann, P. Omling, H.G. Grimmeiss, B.K. Meyer, K.W. Benz, and D. Sinerius, *Phys. Rev. B.* 45, 6247 (1992).
16. J.-H. Yang, L. Shi, L.-W. Wang, and S.-H. Wei, *Sci. Rep.* 6, 21712 (2016).
17. R. Soundararajan, K.G. Lynn, S. Awadallah, C. Szeles, and S.-H. Wei, *J. Electron. Mater.* 35, 1333 (2006).
18. M. Fiederle, C. Eiche, M. Salk, R. Schwarz, K.W. Benz, W. Stadler, D.M. Hofmann, and B.K. Meyer, *J. Appl. Phys.* 84, 6689 (1998).
19. P. Rudolph, A. Engel, I. Schentke, and A. Grochocki, *J. Cryst. Growth* 147, 297 (1995).
20. J.H. Greenberg, V.N. Guskov, V.B. Lazarev, and O.V. Shebershneva, *J. Solid State Chem.* 102, 382 (1993).
21. G. Yang, A.E. Bolotnikov, Y. Cui, G.S. Camarda, A. Hossain, and R.B. James, *J. Cryst. Growth* 311, 99 (2008).
22. J.M. Burst, J.N. Duenow, D.S. Albin, E. Colegrove, M.O. Reese, J.A. Aguiar, C.S. Jiang, M.K. Patel, M.M. Al-Jassim, D. Kuciauskas, S. Swain, T. Ablekim, K.G. Lynn, and W.K. Metzger, *Nat. Energy* 1, 16015 (2016).
23. R. Cohen, V. Lyahovitskaya, E. Poles, A. Liu, and Y. Rosenwaks, *Appl. Phys. Lett.* 73, 1400 (1998).
24. C.H. Swartz, M. Edirisooriya, E.G. LeBlanc, O.C. Noriega, P.A.R.D. Jayathilaka, O.S. Ogedengbe, B.L. Hancock, M. Holtz, T.H. Myers, and K.N. Zaunbrecher, *Appl. Phys. Lett.* 105, 222107 (2014).
25. G. Benz and R. Conradt, *Phys. Rev. B.* 16, 843 (1977).
26. R.K. Ahrenkiel and S.W. Johnston, *Sol. Energy Mater. Sol. Cells* 93, 645 (2009).